Monthly Notices of the ROYAL ASTRONOMICAL SOCIETY

MNRAS **467,** 2430–2444 (2017) doi:10.1093/mnras/stx273
Advance Access publication 2017 February 1

The structure and dynamical evolution of the stellar disc of a simulated Milky Way-mass galaxy

Xiangcheng Ma,[1]★ Philip F. Hopkins,[1] Andrew R. Wetzel,[1,2,3]† Evan N. Kirby,[4] Daniel Anglés-Alcázar,[5] Claude-André Faucher-Giguère,[5] Dušan Kereš[6] and Eliot Quataert[7]

[1]*TAPIR, MC 350-17, California Institute of Technology, Pasadena, CA 91125, USA*
[2]*Carnegie Observatories, 813 Santa Barbara Street, Pasadena, CA 91101, USA*
[3]*Department of Physics, University of California, Davis, CA 95616, USA*
[4]*Department of Astrophysics, MC 249-17, California Institute of Technology, Pasadena, CA 91125, USA*
[5]*Department of Physics and Astronomy and CIERA, Northwestern University, 2145 Sheridan Road, Evanston, IL 60208, USA*
[6]*Department of Physics, Center for Astrophysics and Space Sciences, University of California at San Diego, 9500 Gilman Drive, La Jolla, CA 92093, USA*
[7]*Department of Astronomy and Theoretical Astrophysics Center, University of California Berkeley, Berkeley, CA 94720, USA*

Accepted 2017 January 30. Received 2017 January 30; in original form 2016 August 14

ABSTRACT

We study the structure, age and metallicity gradients, and dynamical evolution using a cosmological zoom-in simulation of a Milky Way-mass galaxy from the Feedback in Realistic Environments project. In the simulation, stars older than 6 Gyr were formed in a chaotic, bursty mode and have the largest vertical scaleheights (1.5–2.5 kpc) by $z = 0$, while stars younger than 6 Gyr were formed in a relatively calm, stable disc. The vertical scaleheight increases with stellar age at all radii, because (1) stars that formed earlier were thicker 'at birth', and (2) stars were kinematically heated to an even thicker distribution after formation. Stars of the same age are thicker in the outer disc than in the inner disc (flaring). These lead to positive vertical age gradients and negative radial age gradients. The radial metallicity gradient is negative at the mid-plane, flattens at larger disc height $|Z|$, and turns positive above $|Z| \sim 1.5$ kpc. The vertical metallicity gradient is negative at all radii, but is steeper at smaller radii. These trends broadly agree with observations in the Milky Way and can be naturally understood from the age gradients. The vertical stellar density profile can be well described by two components, with scaleheights 200–500 pc and 1–1.5 kpc, respectively. The thick component is a mix of stars older than 4 Gyr, which formed through a combination of several mechanisms. Our results also demonstrate that it is possible to form a thin disc in cosmological simulations even with a strong stellar feedback.

Key words: galaxies: abundances – galaxies: evolution – galaxies: formation – cosmology: theory.

1 INTRODUCTION

Gilmore & Reid (1983) first discovered that the vertical stellar density profile in the solar neighbourhood in the Milky Way (MW) can be described by two exponential components with scaleheights ∼300 and ∼1450 pc, respectively, and identified them as the thin disc and the thick disc. Such a two-component profile is also seen in external edge-on disc galaxies (e.g. Yoachim & Dalcanton 2006; Comerón et al. 2011, 2012). However, it remains unclear whether the thin and thick discs are two distinct components or one single structure that varies continuously above the disc plane.

Several mechanisms have been proposed to explain the formation of the thick disc, despite the ambiguity of whether it is a discrete component or not. Some popular scenarios, all motivated by theory or observations, include (1) kinematic heating from a pre-existing thin disc during minor mergers (e.g. Quinn, Hernquist & Fullagar 1993; Hopkins et al. 2008; Kazantzidis et al. 2008; Villalobos & Helmi 2008; Purcell, Kazantzidis & Bullock 2009; Qu et al. 2011), (2) star formation at high redshift from chaotic gas accretion during hierarchical assembly (Brook et al. 2004) or in a turbulent, gas-rich disc (Bournaud, Elmegreen & Martig 2009; Haywood et al. 2013), (3) radial migration of stars from the inner disc to the outer disc

★ E-mail: xchma@caltech.edu
† Caltech-Carnegie Fellow.

(Schönrich & Binney 2009b; Loebman et al. 2011), and (4) accretion of stars from Small Magellanic Cloud-like satellites (Abadi et al. 2003). None the less, it is still unclear which mechanism (or combination of mechanisms) is responsible for the formation of thick discs in the MW and other galaxies.

Thanks to spectroscopic surveys of stars in the MW, such as RAVE (Steinmetz et al. 2006), SEGUE (Yanny et al. 2009), APOGEE (Allende Prieto et al. 2008) and *Gaia*-European Southern Observatory (Gilmore et al. 2012), one can now combine three-dimensional position, velocity and chemical abundance information for large samples (for a recent review, see Rix & Bovy 2013). Many groups have claimed that there are two distinct sub-populations, named α-rich and α-poor stars, as revealed by the gap in the [α/Fe]–[M/H] plane ([M/H] represent total stellar metallicity relative to solar abundance) or the bimodality of the [α/Fe] distribution at fixed [M/H]. These two populations are attributed to the thick and thin discs (e.g. Adibekyan et al. 2013; Anders et al. 2014; Bensby, Feltzing & Oey 2014; Mikolaitis et al. 2014; Nidever et al. 2014; Kordopatis et al. 2015). None the less, some samples show a much less significant gap in the [α/Fe]–[M/H] plane than others (e.g. Mikolaitis et al. 2014; Kordopatis et al. 2015), or no gap at all (e.g. Boeche et al. 2014). Also, in some cases, the bimodality appears in certain α elements but disappears in others (e.g. Bensby et al. 2014; Mikolaitis et al. 2014). Such discrepancies are likely due to large uncertainties in abundance measurements in some studies. The bimodality, if real, implies that the MW may have a hiatus in its star formation history at a high redshift (e.g. Chiappini, Matteucci & Gratton 1997; Brook et al. 2012; Nidever et al. 2014). Also, it is not clear whether such feature is common in other galaxies.

Various groups have confirmed a negative radial metallicity gradient with a slope $\mathrm{d[M/H]/d}R \sim -0.06$ dex kpc^{-1} in MW stars near the disc plane (height $|Z| < 0.5$ kpc), with $\mathrm{d[M/H]/d}R$ gradually flattening above the mid-plane and turning positive at and above $|Z| > 1.5$ kpc (e.g. Cheng et al. 2012; Boeche et al. 2013, 2014; Anders et al. 2014; Hayden et al. 2014; Mikolaitis et al. 2014). A negative vertical metallicity gradient is also found in the MW disc from the mid-plane to $|Z| \sim 3$ kpc, but the slope varies dramatically in the literature (e.g. Carrell, Chen & Zhao 2012; Boeche et al. 2014; Hayden et al. 2014). Hayden et al. (2014) found that the vertical metallicity gradient is steeper at inner Galactocentric radii than at outer radii.

Nevertheless, using the data at a single epoch alone is not sufficient to identify the mechanism for MW-thick disc formation. Cosmological simulations of MW analogues are useful for this problem as they allow one to trace the evolution of the galaxy as well as to understand the underlying implications in the observational data. For example, Stinson et al. (2013) found that older stars tend to have larger scaleheights but shorter scalelengths than younger stars in their MW analogue simulation, which also supported the observationally motivated conjecture in Bovy et al. (2012) that mono-abundance populations (MAPs, stars with certain [Fe/H] and [α/Fe]) are good proxies for single-age populations (see also Matteucci & Brocato 1990; Fuhrmann 1998). Likewise, many authors have also found a two-component disc structure and similar MAP properties in their simulations (e.g. Brook et al. 2012; Bird et al. 2013; Minchev, Chiappini & Martig 2013; Martig, Minchev & Flynn 2014a; Minchev et al. 2017). Most of these simulations show that the thick disc was formed kinematically hot at high redshift, although it has been debated whether heating is important in disc evolution. For instance, Bird et al. (2013) argued that the thick-disc structure is predominantly determined 'at birth', while others suggested that kinematic heating at late times is also significant (e.g. Minchev et al. 2013; Martig, Minchev & Flynn 2014b).

Additionally, Minchev et al. (2013) developed a chemo-dynamical model of disc galaxy evolution, which reconciled the structure, formation history and the variation of metallicity gradients in the disc (see also Minchev, Chiappini & Martig 2014; Minchev et al. 2015). However, Miranda et al. (2016) pointed out that the metallicity gradients in the disc strongly rely on the treatment of (simplified) feedback in these simulations, and only certain recipes produced similar behaviour to the MW in their simulations. Therefore, it is important to include realistic models of the interstellar medium (ISM) and stellar feedback to understand the formation of galactic discs.

In this paper, we study a simulation from the Feedback in Realistic Environments (FIRE; Hopkins et al. 2014) project,[1] which produces a disc galaxy with stellar mass similar to the MW at $z = 0$, to study the structure and abundance pattern of stars in the galactic disc. We present the structure and dynamical evolution of the stellar disc, compare the metallicity gradients and their variation with recent observations and show how the metallicity gradients can be understood from the disc structure. The FIRE project is a suite of cosmological zoom-in simulations with detailed models of the multiphase ISM, star formation and stellar feedback taken directly from stellar evolution models, and it produces reasonable galaxy properties broadly consistent with observations from $z = 0$ to 6, such as the stellar mass–halo mass relation (Hopkins et al. 2014; Feldmann et al. 2016), the Kennicutt–Schmidt law (Orr et al. 2017), neutral hydrogen covering fractions around galaxies at both low and high redshift (Faucher-Giguère et al. 2015, 2016; Hafen et al. 2016), the stellar mass–metallicity relation (Ma et al. 2016), mass-loading factors of galactic winds (Muratov et al. 2015), metal budgets and circumgalactic medium metal content (Muratov et al. 2016), galaxy sizes (El-Badry et al. 2016), and the population of satellite galaxies around MW-mass galaxies (Wetzel et al. 2016). We briefly summarize the simulation in Section 2, present our main results in Section 3, discuss our findings in Section 4, and conclude in Section 5.

We adopt a standard flat Λ cold dark matter cosmology with cosmological parameters $H_0 = 70.2\,\mathrm{km\,s^{-1}\,Mpc^{-1}}$, $\Omega_\Lambda = 0.728$, $\Omega = 1 - \Omega_\Lambda = 0.272$, $\Omega_\mathrm{b} = 0.0455$, $\sigma_8 = 0.807$ and $n = 0.961$, broadly consistent with observations (e.g. Hinshaw et al. 2013; Planck Collaboration XVI 2014).

2 SIMULATION AND METHODS

In this work, we perform a case study using galaxy m12i, a disc galaxy with mass comparable to the MW at $z = 0$, from the FIRE project. We pick this simulation because it has been well studied in previous work (e.g. Hopkins et al. 2014; Anglés-Alcázar et al. 2016; El-Badry et al. 2016; Ma et al. 2017; Muratov et al. 2015, 2016) and has a morphology that is closest to the MW in our suite. A detailed description of the simulations, numerical recipes and physics included is presented in Hopkins et al. (2014, and references therein). We briefly summarize their main features here. The simulation is run using GIZMO (Hopkins 2015), in P-SPH mode, which adopts a Lagrangian pressure–entropy formulation of the smoothed particle hydrodynamics equations, which improves the treatment of fluid-mixing instabilities (Hopkins 2013).

The cosmological 'zoom-in' initial conditions for m12i are adopted from the AGORA project (Kim et al. 2014). The

[1] http://fire.northwestern.edu

zoom-in region is about 1 Mpc in radius at $z = 0$. The initial particle masses for baryons and dark matter are $m_{\rm b} = 5.7 \times 10^4\,{\rm M}_\odot$ and $m_{\rm dm} = 2.8 \times 10^5\,{\rm M}_\odot$, respectively. The minimum force softening lengths for gas and star particles are $\epsilon_{\rm gas} = 14\,{\rm pc}$ and $\epsilon_{\rm star} = 50\,{\rm pc}$ (Plummer-equivalent). The force softening lengths for the gas particles are fully adaptive (Price & Monaghan 2007). The most massive halo in the zoom-in region has a halo mass of $M_{\rm halo} = 1.4 \times 10^{12}\,{\rm M}_\odot$ and a stellar mass around $M_* = 6 \times 10^{10}\,{\rm M}_\odot$ at $z = 0$.

In our simulation, gas follows a molecular-atomic-ionized cooling curve from 10 to 10^{10} K, including metallicity-dependent fine-structure and molecular cooling at low temperatures and high-temperature metal-line cooling followed species-by-species for 11 separately tracked species (H, He, C, N, O, Ne, Mg, Si, S, Ca and Fe; see Wiersma, Schaye & Smith 2009a). At each time-step, the ionization states and cooling rates are determined from a compilation of CLOUDY runs, including a uniform but redshift-dependent photoionizing background tabulated in Faucher-Giguère et al. (2009) and approximate models of photoionizing and photoelectric heating from local sources. Gas self-shielding is accounted for with a local Jeans-length approximation, which is consistent with the radiative transfer calculations in Faucher-Giguère et al. (2010).

We follow the star formation criteria in Hopkins, Narayanan & Murray (2013) and allow star formation to take place only in locally self-gravitating, self-shielding/molecular gas that also exceeds a hydrogen number density threshold $n_{\rm th} = 5\,{\rm cm}^{-3}$. Stars form on the local free-fall time when the gas meets these criteria and there is no star formation elsewhere. Once a star forms, it inherits the metallicity of each tracked species from its parent gas particle. Every star particle is treated as a single stellar population with known mass, age and metallicity, assuming a Kroupa (2002) initial mass function from 0.1 to 100 $\rm M_\odot$. All the feedback quantities, including ionizing photon budgets, luminosities, supernovae (SNe) rates, mechanical luminosities of stellar winds, etc., are then directly tabulated from the stellar population models in STARBURST99 (Leitherer et al. 1999). We account for several different stellar feedback mechanisms, including (1) local and long-range momentum flux from radiative pressure, (2) energy, momentum, mass and metal injection from SNe and stellar winds, and (3) photoionization and photoelectric heating. We follow Wiersma et al. (2009b) and account for metal production from Type II SNe, Type Ia SNe and stellar winds using the metal yields in Woosley & Weaver (1995), Iwamoto et al. (1999) and Izzard et al. (2004), respectively. The rates of Type II and Type Ia SN are separately computed from STARBURST99 and following Mannucci, Della Valle & Panagia (2006), respectively.

We note that the Mg yield from Type II SN in Woosley & Weaver (1995) is ∼0.4 dex lower than typical values in more recent models (e.g. Nomoto et al. 2006). Therefore, we manually add 0.4 dex to all Mg abundances in our simulation to compare with observations more accurately. This will have little effect on global galaxy properties, since Mg is not an important coolant (it is simply a 'tracer species'). Also, the total number of Type Ia SNe calculated from Mannucci et al. (2006) is lower than that derived from Maoz, Sharon & Gal-Yam (2010) by a factor of a few for a stellar population older than 1 Gyr; this may lead to predictions of lower Fe, but we cannot simply renormalize the Fe abundances in the simulation. We do not include a sub-resolution metal diffusion model in the simulation; all mixing above the resolution scale is explicitly resolved.

We use the Amiga Halo Finder (AHF; Knollmann & Knebe 2009) to identify haloes in the simulated box, where we adopt the time-dependent virial overdensity from Bryan & Norman (1998). In this work, we only study the most massive (hence best-resolved) halo in the zoom-in region, which hosts a disc galaxy of very similar properties to the MW at $z = 0$. At each epoch, we define the galactic Centre at the density peak of most stars and find the stellar half-mass radius as the radius within which the stellar mass equals to half of the stellar mass within 0.1 virial radius. Then the Z-axis is defined to be aligned with the total angular momentum of the gas within 5 stellar half-mass radii. In this paper, we will primarily focus on the stellar component. We do not perform a kinematic decomposition for the stellar content, but take all star particles in the analysis to form an unbiased sample.

Table 1. A list of symbols used in this paper.

Symbol	Description
z	Redshift
$t_{\rm lookback}$	Lookback time
Age	Stellar age at $z = 0$
X, Y, Z	Cartesian coordinates
R	Galactocentric radius
$\lvert Z\rvert$	Height from the mid-plane
[M/H]	Total metallicity (relative to solar)
[Fe/H]	Fe abundance (relative to solar)
[Mg/Fe]	Mg to Fe abundance ratio (relative to solar)

A list of symbols used in this paper and their descriptions are presented in Table 1. In the rest of this paper, we always mean the $z = 0$ age when we quote stellar ages and will predominantly use lookback time ($t_{\rm lookback}$) when referring to an epoch in the simulation. In Table 2, we list the conversion between lookback time and redshift at selected epochs for reference.

3 RESULTS

3.1 General picture

At high redshifts, the galaxy accretes gas rapidly and undergoes multiple mergers, producing violent, bursty star formation, until a final minor merger finished at $z \sim 0.7$ (corresponding to a lookback time of $t_{\rm lookback} \sim 6\,{\rm Gyr}$). Since then, a calm, stable gas disc was formed and maintained, with stars forming in the disc at a nearly constant rate ($\sim 7\,{\rm M}_\odot\,{\rm yr}^{-1}$, integrated across the entire disc) regulated by stellar feedback.

The top panel in Fig. 1 illustrates the stellar morphologies at $z = 0$ for stars in the galaxy in six different $z = 0$ age intervals. The top and bottom panels show the stellar surface density viewed face-on and edge-on, respectively. The thickness increases with stellar age, from a thin disc-like structure to more spheroidal morphology, broadly consistent with the MW (Bovy et al. 2012) and other simulations (e.g. Brook et al. 2012; Bird et al. 2013; Minchev et al. 2013; Stinson et al. 2013; Martig et al. 2014a). On the other hand, the radial morphology first shrinks with increasing age ('inside-out' growth), but then becomes less concentrated for ages greater than 8 Gyr, leaving intermediate-age stars (age $\sim 6\,{\rm Gyr}$) the most radially concentrated. This is in contrast with the results in Bovy et al. (2012) and other simulations where the scalelength decreases monotonically with a stellar age (oldest stars have the smallest scalelengths). This directly owes to a minor merger in the simulation around lookback time $t_{\rm lookback} \sim 6\,{\rm Gyr}$ ($z \sim 0.7$), which drove a concentrated nuclear starburst. Afterwards, the disc formed inside-out.

The middle panel in Fig. 1 shows the stellar morphologies for the same stars shown in the top panel (divided into the same $z = 0$ age intervals), but viewed at the epoch when they just formed (labelled by a lookback time). In other words, we trace the galaxy back to these epochs, and show the young stars in the main

Table 2. Lookback time versus redshift.

Lookback time ($t_{\rm lookback}$, in Gyr)	0	1	2	3	4	5	6	7	8	10
Redshift [z]	0	0.076	0.162	0.258	0.369	0.497	0.649	0.834	1.068	1.812

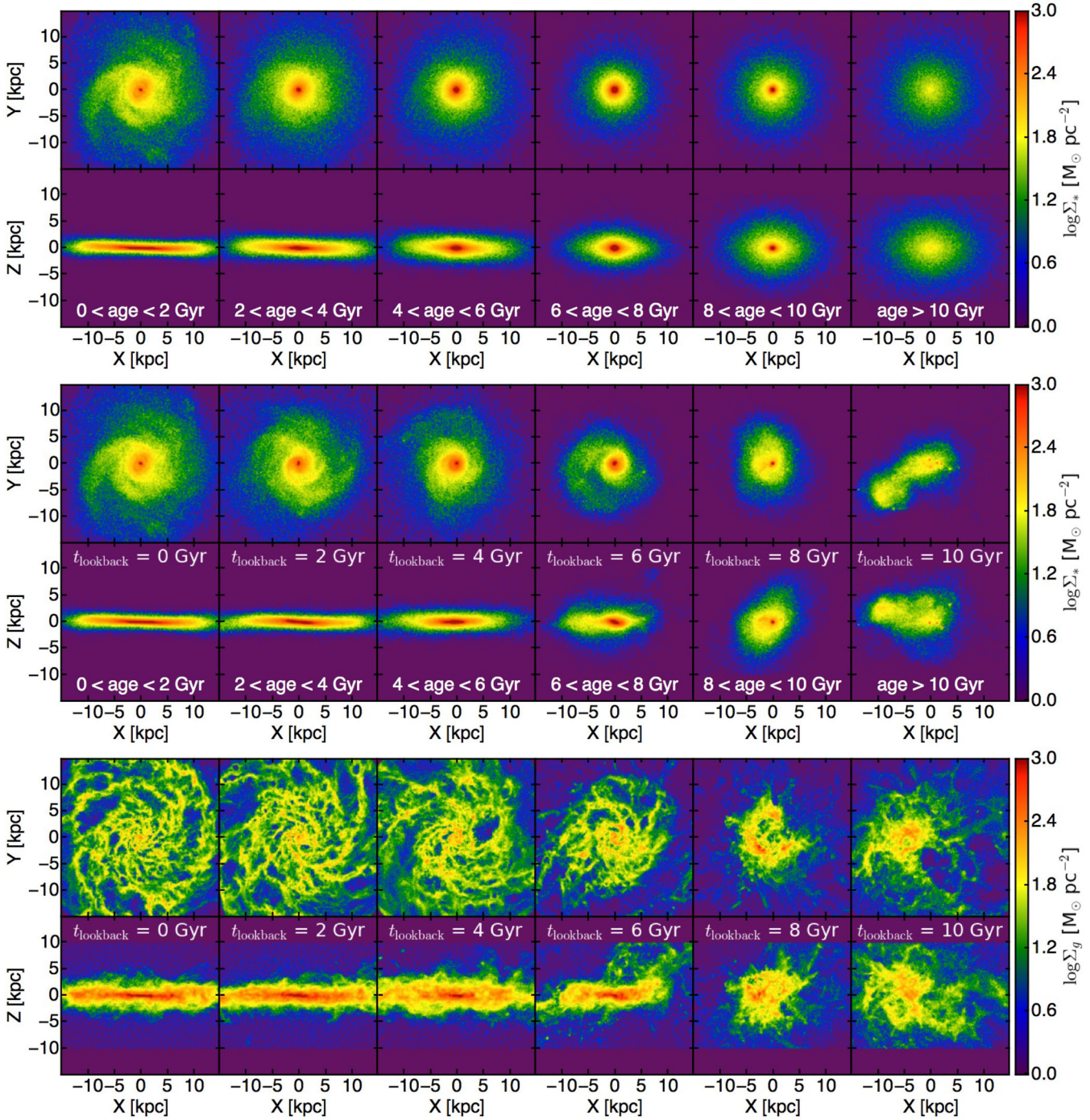

Figure 1. Top panel: morphology of stars in different age intervals at $z = 0$. The thickness increases with stellar age, but the scalelength first decreases with stellar age in $0 <$ age < 6 Gyr and then increases in age > 8 Gyr, leaving stars of age ~ 6 Gyr the most radially concentrated (owing to a merger-driven nuclear starburst about this time). Middle panel: morphology of the same stars from each $z = 0$ age interval in the top panel, but viewed at the epoch when they just formed (labelled by a lookback time) in the galaxy progenitor. Stars younger than 6 Gyr at $z = 0$ were formed in a relatively calm disc. Stars older than 8 Gyr at $z = 0$ were formed in a violent, bursty mode, and relax by $z = 0$. Bottom panel: morphology of gas, viewed at the same epochs as in the middle panel. At early time, the gas is highly irregular and chaotic. By $t_{\rm lookback} \sim 6$ Gyr ($z \sim 0.7$), the gas eventually formed a disc.

progenitor galaxy at that time. Stars older than 8 Gyr were born to be a chaotic, non-disc-like structure. For illustrative purposes, we also show gas morphologies at the same epochs in the bottom panel in Fig. 1. During the early stage of galaxy assembly when the stellar mass was sufficiently low, this galaxy experienced bursty, chaotic star formation (Sparre et al. 2017). Starbursts drive bursts of gas outflows with high efficiency (Muratov et al. 2015), and the bursty outflows, in turn, modify the potential and cause radial migration of stars, resulting in radial expansion and quasi-spherical morphology for stars older than 8 Gyr (El-Badry et al. 2016). A gas disc is formed by $t_{\rm lookback} \sim 6$ Gyr ($z \sim 0.7$). Below $t_{\rm lookback} \lesssim 6$ Gyr, star formation takes place in a relatively calm mode, with stars forming in a relatively stable disc at a rate self-regulated by feedback, and there are no longer large-scale outflows (Muratov et al. 2015; Anglés-Alcázar et al. 2016). Hayward & Hopkins (2017) proposed an analytic model and argued that such bursty-to-calm transition is expected in massive galaxies at late times, due to the change of ISM structure at low gas fractions.

We estimate the fraction of stars that comes from mergers or tidally disrupted satellites, i.e. stars formed outside the main progenitor galaxy, using the particle tracking technique developed by and presented in Anglés-Alcázar et al. (2016). We find that only $\lesssim$10 per cent of the stellar mass in the $z = 0$ galaxy was formed *ex situ* and this contribution is only significant far above the galactic plane ($|Z| \gtrsim 5$ kpc). For example, during the last minor merger at $t_{\rm lookback} \sim 6$ Gyr ($z \sim 0.7$), the passing-by satellite has been tidally disrupted and its stars are re-distributed in the diffuse halo. Within the galactic disc, which we select to be in galactocentric radius $R = 4$–14 kpc and $|Z| < 3$ kpc (to exclude bulge and halo stars), stars that were formed *ex situ* contribute no more than a few per cent of the stellar mass, so we will ignore them in the analysis below.

3.2 Disc structure

One common argument for the presence of a thick disc in the MW and nearby disc galaxies is that the stellar density profile along the $|Z|$-direction cannot be well described by a single-component profile:

$$\rho_*(|Z|) = \rho_*(0)\,\mathrm{sech}^2\left(\frac{|Z|}{2Z_H}\right), \quad (1)$$

where Z_H is the scaleheight, but requires a second component

$$\rho_*(|Z|) = \rho_{*,1}(0)\,\mathrm{sech}^2\left(\frac{|Z|}{2Z_{H,1}}\right) + \rho_{*,2}(0)\,\mathrm{sech}^2\left(\frac{|Z|}{2Z_{H,2}}\right) \quad (2)$$

(e.g. Gilmore & Reid 1983; Yoachim & Dalcanton 2006; Comerón et al. 2011, 2012). In Fig. 2, we show the vertical stellar density profile $\rho_*(|Z|)$ at $R \sim 8$ kpc in our simulation (black dots) at $z = 0$ and fit it with a single-component profile (grey dotted line) and a two-component profile (black dashed line), respectively. The dark green and brown lines show the thin and thick components, respectively.

We find that a two-component profile provides a much better fit than a single-component profile. The two components, which we refer as the 'thin' and 'thick' discs, have scaleheights of $Z_{H,1} \sim 300$ pc and $Z_{H,2} \sim 1.1$ kpc, respectively, close to the observed MW-disc scaleheights around the solar neighbourhood (300 and 1450 pc; e.g. Gilmore & Reid 1983). Derived from the profile fitting, the thick disc component contributes 36 per cent of the stellar mass at $R = 8$ kpc, broadly in agreement with measurements of nearby edge-on disc galaxies (e.g. Yoachim & Dalcanton 2006) as well as other simulations (e.g. Brook et al. 2012; Bird et al. 2013; Minchev et al. 2013). Note that this is far greater than the fraction of stars that were formed *ex situ*, which is $\lesssim$5 per cent at $R = 8$ kpc, so the 'thick disc' in our simulation does not originate from accreted satellite galaxies.

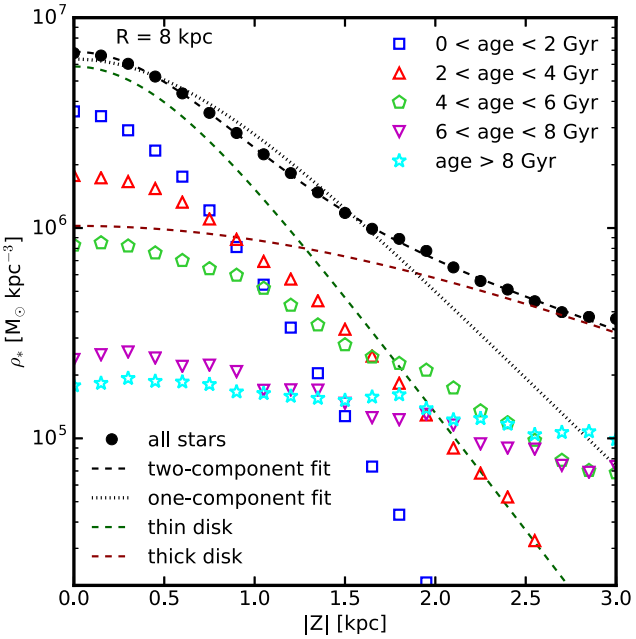

Figure 2. Vertical stellar density profile $\rho_*(|Z|)$ at $R = 8$ kpc (black points) in the simulation at $z = 0$. The density profile cannot be well described by a single-component profile (equation 1, black dotted line), while a two-component profile provides a good fit (equation 2, black dashed line). The dark green and brown dashed lines show the thin- and thick-disc profiles from the fitting. The 'thin' and 'thick' discs have scaleheights of 300 pc and 1.1 kpc, respectively, close to the MW scaleheights around the solar neighbourhood (300 and 1450 pc; e.g. Gilmore & Reid 1983). The 'thick disc' contributes 36 per cent of the total stellar mass around $R = 8$ kpc. Note that the stellar densities, thin- and thick-disc scaleheights, and the mass fraction of the thick disc in our simulation are in good agreement with observations and other simulations in the literature. The open symbols show the density of stars in different age intervals. Stars younger than 4 Gyr contribute more than 90 per cent of the mass in the 'thin disc', while the 'thick disc' is made almost entirely of stars older than 4 Gyr.

In Fig. 2, we further decompose the density profile into five bins according to stellar age (open symbols). Qualitatively, the thickness of stars increases with age, with the youngest stars being most concentrated to the mid-plane and the oldest stars being most vertically extended. This is consistent with the visualization shown in Fig. 1. We find that over 90 per cent of the mass in the 'thin disc' is contributed by stars younger than 4 Gyr, while the 'thick disc' is made of stars older than 4 Gyr. Note that our thin-to-thick disc decomposition is purely based on the mass density at this point. In Section 4.1, we will further discuss the formation mechanisms of both components.

Stars in each age interval in Fig. 2 can be well described by a single-component profile from equation 1 (see also, e.g. Bird et al. 2013; Minchev et al. 2013, 2015; Martig et al. 2014a). In Fig. 3, we further show Z_H as a function of R for stars in all five age intervals. Only $R = 4$–14 kpc is shown to minimize contamination from the bulge component, which is important within $R < 4$ kpc. Stars older than 8 Gyr have very large scaleheights ($Z_H > 1.5$ kpc), since they were formed during the chaotic phase and have relaxed to be quasi-spherical by $z = 0$. Stars younger than 6 Gyr have considerably smaller scaleheights, since they were formed in a disc.

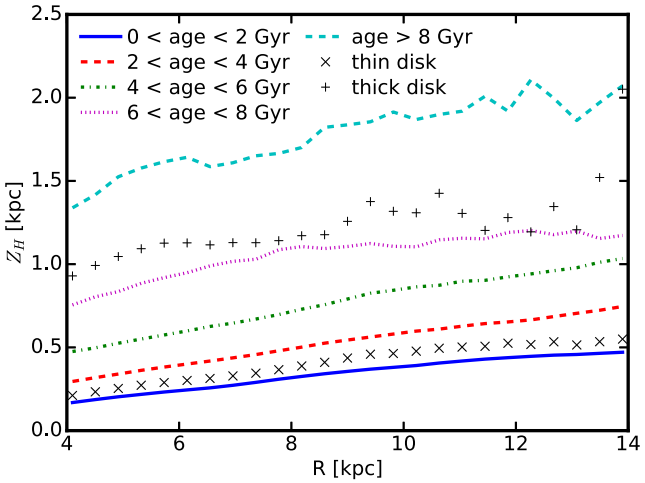

Figure 3. Scaleheights of stars in five age intervals, as a function of galactocentric radius in the disc. Each population can be well described by a single-component profile from equation (1). At fixed radius, Z_H increases with stellar age. For a given population, Z_H increases with R. The cross and plus symbols show the scaleheights of the thin- and thick-disc component, respectively. At all radii, the 'thin disc' has a scaleheight close to that of stars younger than 4 Gyr.

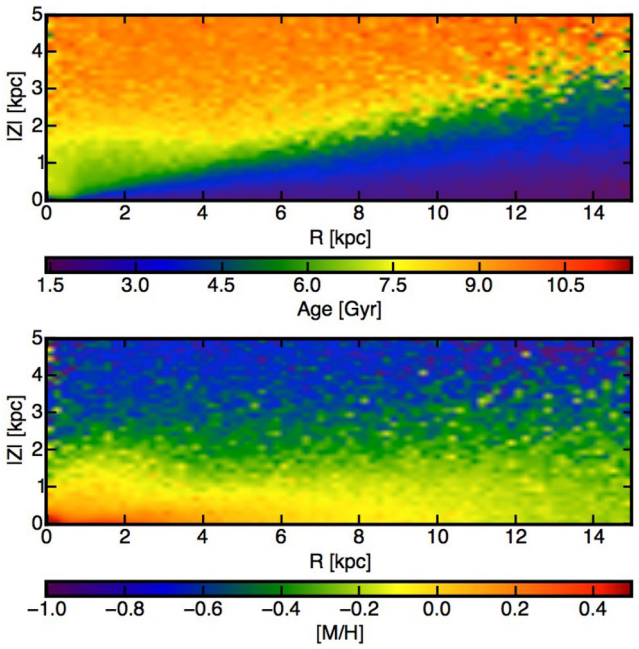

Figure 4. Top panel: median stellar age as a function of R and $|Z|$. The median stellar age naturally follows the disc structure. At fixed radius, stellar age increases with $|Z|$. Above the mid-plane, the stellar age decreases with R due to disc flaring. Bottom panel: stellar metallicity in the disc. [M/H] is higher at the inner disc and near the mid-plane than at the outer disc and large heights.

Even for these stars, the scaleheights increase with stellar age at any radius. For example, the scaleheights of stars with age 4–6 Gyr are larger than those of stars with age $<$ 2 Gyr by a factor of 2. Note that this is equivalent to the observed age–velocity dispersion relation (e.g. Nordström et al. 2004), since the vertical velocity dispersion is proportional to the disc thickness as expected from the disc equilibrium. For comparison, we also show the scaleheights of the 'thin' and 'thick' discs as a function of galactocentric radius (black cross and plus symbols). At all radii, the 'thin disc' scaleheights are comparable to those of stars younger than 4 Gyr ($Z_{H,1}$ = 200–500 pc), while the 'thick disc' represents a median stellar age of 8 Gyr ($Z_{H,2}$ = 1–1.5 kpc). Moreover, the disc is flaring for stars younger than 6 Gyr – the scaleheight increases with R, with Z_H being a factor of 2 larger at R = 14 kpc than that at $R = 4$ kpc. The disc flaring broadly agrees with observations in the MW stellar disc (e.g. Momany et al. 2006; Kalberla et al. 2014; López-Corredoira & Molgó 2014; Bovy et al. 2016).

3.3 Age and metallicity gradients

In Fig. 4, we show the median stellar age as a function of galactocentric radius R and height $|Z|$ (upper panel) for R = 0–15 kpc and $|Z|$ = 0–5 kpc in our simulation at $z = 0$. At each radius, the median stellar age increases with $|Z|$, resulting in a significant positive vertical age gradient in the disc. Moreover, there is also a moderate negative radial age gradient above the mid-plane, as the median stellar age decreases with R at fixed $|Z|$. These features naturally follow the disc structure presented above: (1) differential scaleheights of stars in different age intervals, and (2) the disc flaring for any single-age stellar population. These results are in line with predictions from Minchev et al. (2015) and observations from Martig et al. (2016). In Fig. 4, we also show the mass-weighted mean stellar metallicity as a function of R and $|Z|$ (bottom panel). Qualitatively, the stellar metallicity is higher at the inner disc and near the mid-plane than at the outer disc and large heights.

In Fig. 5, we further show the radial metallicity gradient d[M/H]/dR as a function of height $|Z|$ (left-hand panel) and vertical metallicity gradient d[M/H]/d$|Z|$ as a function of galactocentric radius R (right-hand panel). The black dashed lines show the values measured in the $z = 0$ snapshot of our simulation. The radial metallicity gradient at a certain $|Z|$ is measured using stars in a layer of thickness $\Delta|Z| = 0.5$ kpc and by fitting the radial metallicity profile from R = 4 to 14 kpc with a simple linear function. For vertical metallicity gradients, we use stars in annuli of $\Delta R = 1$ kpc and fit the vertical metallicity profile from $|Z| = 0$ to 2.5 kpc with a linear function. We take all star particles into account.

In Fig. 5, we also compare our results with published radial and vertical metallicity gradients measured from different samples of MW stars in the literature (Carrell et al. 2012; Cheng et al. 2012; Anders et al. 2014; Boeche et al. 2014; Hayden et al. 2014). The horizontal error bars show the R or $|Z|$ interval where the metallicity gradient is measured. Our simulation is qualitatively consistent with observations, despite the fact that the slopes are not identical – d[M/H]/d$R = -0.03$ dex kpc^{-1} at $|Z| < 0.5$ kpc is shallower than the canonical MW value of -0.06 dex kpc^{-1}, but is close or slightly steeper than that of -0.02 dex kpc^{-1} in M31 (e.g. Gregersen et al. 2015). It is difficult to know whether this discrepancy is meaningful without a large, statistically significant sample (both simulated and observed). We find that the radial gradient is negative and the steepest near the mid-plane, gradually flattens, and finally becomes positive above $|Z| \gtrsim 1.5$ kpc, as observed in the MW (e.g. Cheng et al. 2012; Anders et al. 2014; Boeche et al. 2014) and predicted in other simulations (e.g. Minchev et al. 2014, 2015). The vertical gradient is negative at any radius between $R = 4$ and 14 kpc, but is steeper at inner radii. This trend is qualitatively consistent with observations in Hayden et al. (2014).

To understand why the metallicity gradients have such behaviour, in Fig. 6 we break down the radial (top panels) and vertical (bottom panels) metallicity profiles into four age intervals: age $<$ 2 Gyr (blue

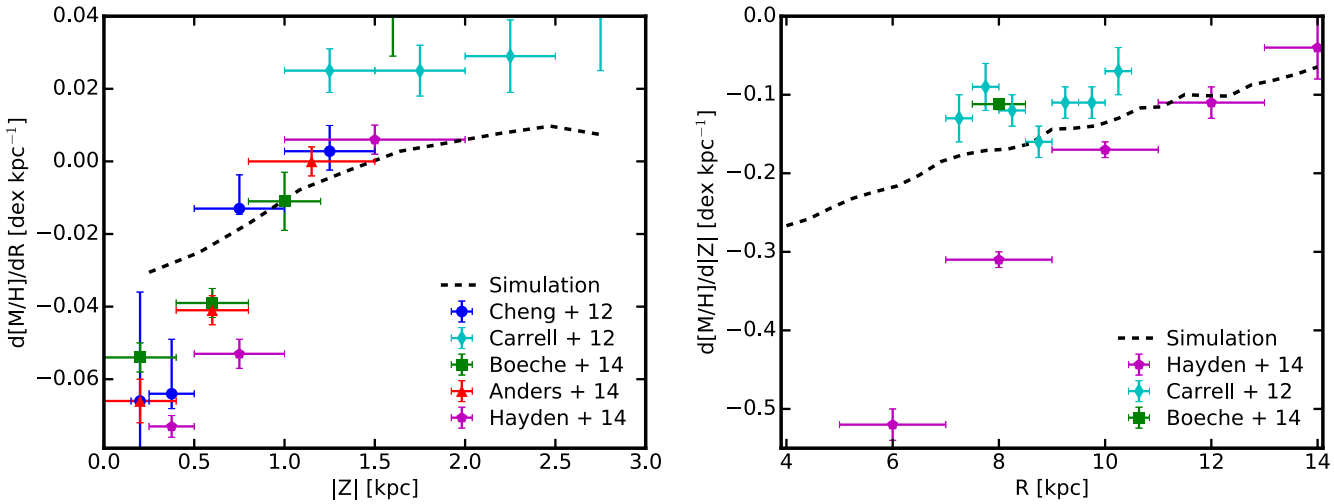

Figure 5. Left-hand panel: radial metallicity gradient d[M/H]/dR as a function of height $|Z|$. Right-hand panel: vertical metallicity gradient d[M/H]/d$|Z|$ as a function of galactocentric radius R. d[M/H]/dR is negative at the mid-plane, gradually increases with $|Z|$ and eventually becomes positive above $|Z| \sim 1.5$ kpc. d[M/H]/d$|Z|$ is negative at all radii, but is stronger at smaller radii. These trends are qualitatively consistent with observations in the MW disc. A number of observations are shown, including Cheng et al. (2012), Carrell et al. (2012), Boeche et al. (2014), Anders et al. (2014) and Hayden et al. (2014).

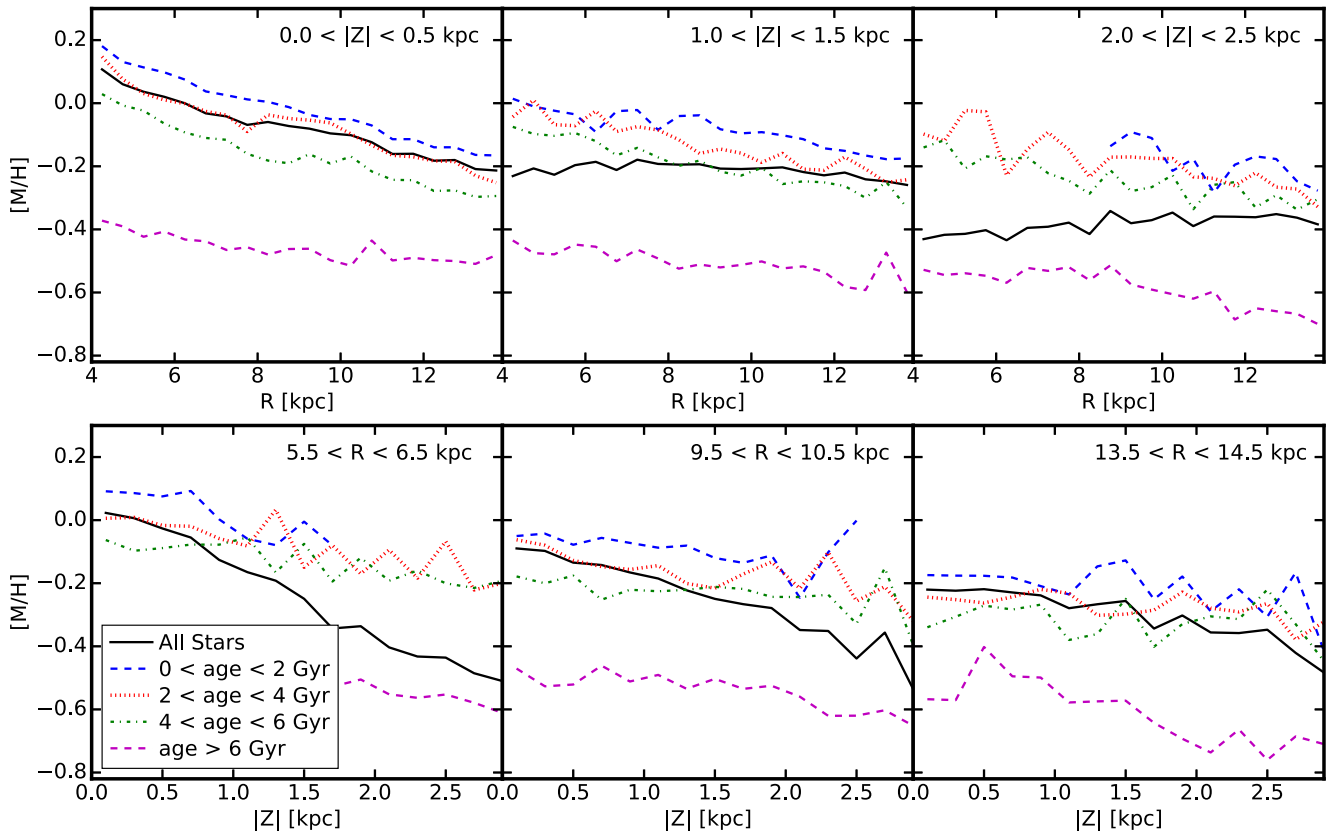

Figure 6. Top panel: radial metallicity profile in layers with $|Z| = 0$–0.5, 1.0–1.5 and 2.0–2.5 kpc. Bottom panel: vertical metallicity profile at radii $R = 6, 10$ and 14 kpc. We show the metallicity profiles for all stars (black solid lines) as well as in bins of different stellar ages. The flattening and inversion of the radial metallicity gradient at high $|Z|$ follows the negative age gradient at these heights. The steepening of the vertical metallicity gradient at smaller radii results from a stronger age gradient. The stellar age gradient is a natural consequence of disc structure. These results are in line with the predictions in Minchev et al. (2014, fig. 10).

dashed lines), 2 < age < 4 Gyr (red dotted lines), 4 < age < 6 Gyr (green dash–dotted lines) and age > 6 Gyr (magenta dashed lines). The black lines show the metallicity profile of all stars. To leading order, metallicity is a proxy of stellar age, with young stars being more metal-enriched than old stars (also see Section 4.3). The top panels in Fig. 6 show the radial metallicity profiles from $R = 4$ to 14 kpc in three layers: $0 < |Z| < 0.5$ kpc, $1.0 < |Z| < 1.5$ kpc and $2.0 < |Z| < 2.5$ kpc. The flattening and inversion of the radial metallicity gradient can be naturally understood from the negative age gradient at large heights. For example, in the $2.0 < |Z| < 2.5$ kpc

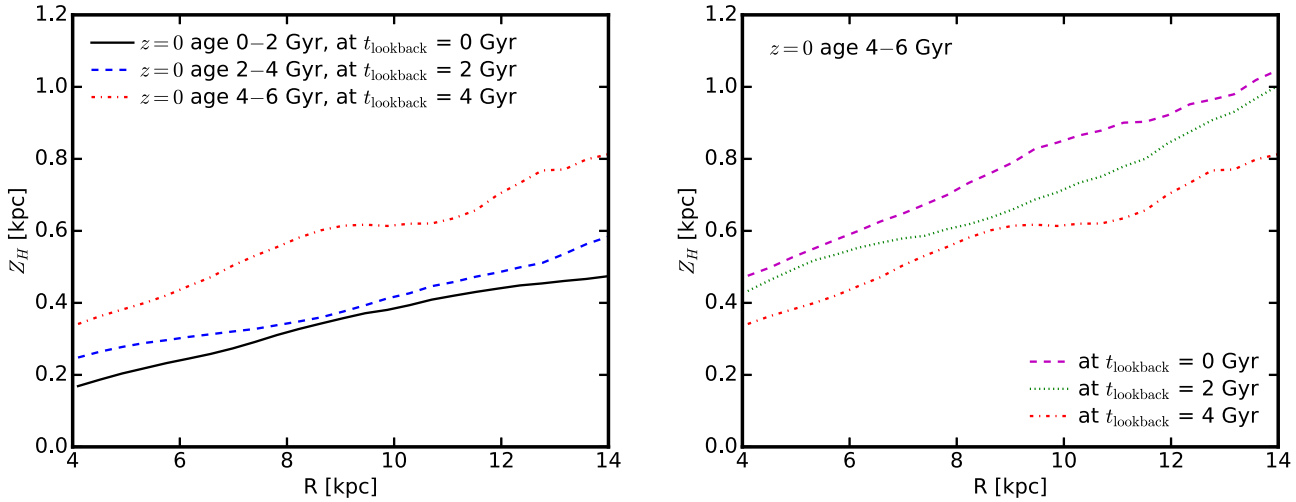

Figure 7. Left-hand panel: scaleheights of stars in three $z = 0$ age intervals (0–2, 2–4 and 4–6 Gyr), measured at the epoch when the stars formed (labelled by a lookback time). Right-hand panel: the evolution of scaleheights for stars of age 4–6 Gyr at $z = 0$, as they would be observed at three different epochs (labelled by a lookback time) after their formation. Stars formed at an early epoch were born in a thicker disc than those formed at later times, because the star-forming disc was more gas-rich and therefore turbulent. The scaleheights of those populations then increase with time due to kinematic heating.

layer, old, metal-poor stars dominate at $R = 4$ (where the disc scaleheights of young stars are small, i.e. $Z_H \sim 0.3$ kpc), while younger, more metal-enriched stars take over at much larger radius (where the young stellar disc is thicker in absolute units, e.g. $Z_H \sim 1$ kpc at $R = 14$ kpc). This leads to an overall positive radial metallicity gradient at this fixed height. Note that our interpretations here agree well with the chemo-dynamical model in Minchev et al. (2014, fig. 10). The bottom panels in Fig. 6 show the vertical metallicity profile at $R = 6$, 10 and 14 kpc, respectively. The reasons why the vertical metallicity gradient flattens at large radius are twofold: (1) The metallicity of young stars is lower at larger radius than at small radius, and (2) the age gradient is much weaker at larger radius.

The negative radial metallicity gradient for stars younger than 6 Gyr (those formed in a disc) near the mid-plane is inherited from the parent star-forming gas disc (Ma et al. 2017). A negative radial metallicity gradient is expected from the co-evolution between the gas disc and stellar disc (e.g. Ho et al. 2015). In short, suppose a pure gas disc has formed with an exponential surface density profile and begun to form stars. The star formation efficiency is higher at the inner disc than at the outer disc according to the observed Kennicutt–Schmidt law (Kennicutt 1998). Under the local closed-box assumption, the inner disc would be enriched more rapidly than the outer disc, leading to a negative radial metallicity gradient in the disc. None the less, the slope of such a gradient can be affected by disc scalelength, radial inflow and mixing, disc pre-enrichment, etc. A comprehensive analysis of the radial metallicity gradient and its dependence on galaxy properties with a larger sample of simulations is presented in a companion study (Ma et al. 2017).

3.4 Dynamical evolution of the stellar disc

In Section 3.2, we show that even for stars that are initially formed in a disc (i.e. stars younger than age ~ 6 Gyr by $z = 0$), by $z = 0$, their scaleheight increases with stellar age at all radii (Fig. 3). To explain this, we first explore the scaleheights of stars at the time when they just formed. In the left-hand panel in Fig. 7, we show the scaleheights for stars in three $z = 0$ age intervals: 0–2, 2–4 and 4–6 Gyr, but measured just after their formation time (labelled by a lookback time). In other words, these stars are younger than 2 Gyr at the time we measure their scaleheights. The newly formed stars inherit the scaleheights and velocity dispersion from the cold star-forming gas in the disc where they were born. In general, stars formed earlier (which are older today) were born with larger scaleheights than stars formed at late times. For example, stars with $z = 0$ age interval 4–6 Gyr (formation time at $t_{\rm lookback} = 4$ Gyr) were born with a scaleheight of $Z_H \sim 0.4$ (0.8) kpc at $R = 4$ (14) kpc at this epoch, larger by a factor of $\sim$2 compared to the 'at birth' scaleheights of stars formed at $z = 0$. This naturally follows the evolution of the gas disc, because the thickness of a star-forming disc, where self-regulation by feedback yields a Toomre parameter $Q \sim 1$, is proportional to its gas fraction (e.g. Thompson, Quataert & Murray 2005; Faucher-Giguère, Quataert & Hopkins 2013), which is higher at early times.

We now examine how the scaleheight evolves over time. In the right-hand panel in Fig. 7, we show the scaleheights at three post-formation epochs (labelled by a lookback time), for stars in the $z = 0$ age interval 4–6 Gyr. At all radii, the scaleheight increases by $\sim$30 per cent (or $\sim$0.2 kpc in absolute units) over 4 Gyr from their formation time to $z = 0$. During the same period, the vertical velocity dispersion has also increased consistently. Our simulation shows that kinematic heating plays a non-negligible role in the formation of the thick disc, in line with the predictions in Minchev et al. (2013) and Martig et al. (2014b), but in contrast with the argument in Bird et al. (2013).

Several mechanisms have been proposed to cause such kinematic heating, including (1) bars and spiral arms (e.g. Sellwood & Carlberg 1984; Minchev & Quillen 2006; Saha, Tseng & Taam 2010; Faure, Siebert & Famaey 2014; Yurin & Springel 2015; Grand et al. 2016), (2) radial migration (e.g. Schönrich & Binney 2009b; Loebman et al. 2011; however, see e.g. Minchev et al. 2012; Vera-Ciro et al. 2014; Grand et al. 2016), (3) perturbation of satellites and sub-haloes (e.g. Quinn et al. 1993; Kazantzidis et al. 2008; Purcell et al. 2009; Gómez et al. 2013) and (4) scattering by giant molecular clouds (GMCs) or star clusters (e.g. Spitzer & Schwarzschild 1951, 1953; Aumer, Binney & Schönrich 2016). In a cosmological context, these mechanisms are usually combined and difficult to isolate in practice. For example, gravitational perturbation of satellites can induce bars and spiral arms (e.g. Purcell

et al. 2011), which further result in kinematic heating and radial migration (Lynden-Bell & Kalnajs 1972). Scattering by massive GMCs is also needed to redistribute the energy between planar and vertical motions (Carlberg 1987). In our simulation, the increase of disc thickness and velocity dispersion is roughly a linear function of time, indicating that spiral arms may be the dominant heating mechanism, as suggested by an analysis of a large sample of disc galaxy simulations (Grand et al. 2016).

The flaring of the stellar disc is present 'at birth' and preserved during kinematic heating. At their formation time, stars inherited the flaring of their parent gas disc, which is likely to be a natural consequence of hydrostatic equilibrium in a galactic potential (e.g. Olling 1995; O'Brien, Freeman & van der Kruit 2010; Allaert et al. 2015), although disc flaring may also be induced and enhanced by mergers (e.g. Bournaud et al. 2009; Purcell et al. 2011) and radial migration (e.g. Minchev et al. 2012).

4 DISCUSSION

In this section, we discuss some observational and theoretical implications of our simulation. Although our analysis in Section 3 is based on a single simulation, preliminary analysis of several other MW-mass disc galaxy simulations indicates that the disc structure and dynamic evolution are similar in other systems, including one using an eight times higher mass resolution from Wetzel et al. (2016, see Appendix A for more details), despite the fact that these simulations are run with a different hydrodynamic method and slightly modified numerical implementations of the feedback model (the FIRE-2 code, see Hopkins et al., in preparation). This suggests that the results presented in Section 3 are typical in similar systems and insensitive to resolution and numerical method, as implied also by the good agreement between our results and many other simulations (e.g. Brook et al. 2012; Minchev et al. 2013, 2014; Martig et al. 2014a,b). This is expected since our key results are derived from global processes and can be understood with simple analytic models, including the following: (1) Star formation is bursty at high redshift and becomes relatively stable at late times, (2) the thickness of the star-forming gas disc decreases at low gas fraction, and (3) the kinematic heating is continuously present from spiral structure, bars, GMCs, etc. Therefore, they should be independent of the subtle difference in the numerical details of small-scale physics. A comprehensive analysis on disc morphology and its dependence on galaxy formation history using an enlarged sample of galaxies will be the subject of a future study.

4.1 The thin and thick discs

In Section 3.2, we show that the vertical stellar density profile in the simulation can be well described by a two-component function (Fig. 2), which we refer to as the traditional thin disc ($Z_H \sim 200$–500 pc) and thick disc ($Z_H \sim 1$–1.5 kpc; Gilmore & Reid 1983). In terms of mass density, the thin and thick discs in our simulation can be roughly divided into stars younger and older than 4 Gyr, respectively.

We first discuss the formation mechanisms of the thick disc. In Fig. 8, we show the scaleheights as a function of stellar age at three radii $R = 5$, 9 and 13 kpc. The cross and plus symbols represent the scaleheights of the thin and thick components, respectively, as obtained from profile fitting. The vertical dotted line located at 4 Gyr illustrates the separation of the thin and thick discs. The thick disc contains two distinct populations. First, about two-third of the stars in the thick disc are older than 6 Gyr (formation redshift $z \gtrsim 0.7$).

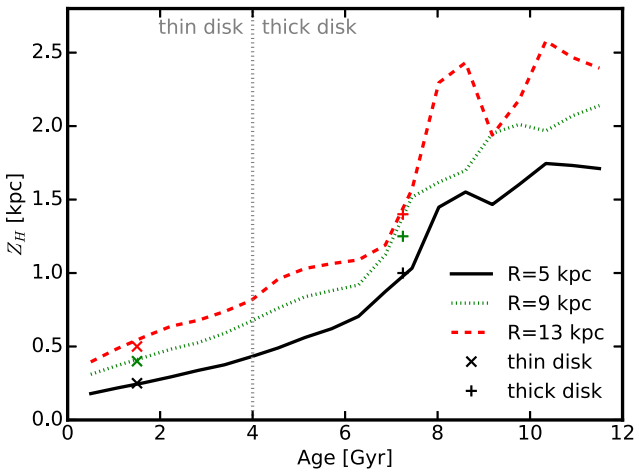

Figure 8. Scaleheights as a function of stellar age at $R = 5$, 9 and 13 kpc. The cross and plus symbols show the scaleheights of the 'thin' and 'thick' components obtained from the profile fitting (e.g. see Fig. 2) at three radii, but we intentionally select their x-coordinates to match the curve. At all radii, the scaleheights increase dramatically above stellar age 6 Gyr, since these stars were formed in a chaotic, bursty mode. In terms of mass density, the thin and thick discs can be separated by stars younger and older than 4 Gyr, as illustrated by the vertical dotted line. The thick disc defined in this way contains two distinct populations of stars: (1) stars older than 6 Gyr, which were formed in the chaotic, bursty mode, and (2) stars in 4–6 Gyr age interval that were formed in a gas-rich disc, and kinematically heated after their formation. Note that the gas disc evolved smoothly during the past 6 Gyr, so there is no sharp transition at 4 Gyr ago when the thin disc at $z = 0$ started to form.

These were formed during the chaotic, bursty phase in the galaxy progenitor (Fig. 1). This agrees with the picture proposed in Brook et al. (2004). These stars have very large scaleheights, as shown in Fig 8. Secondly, the other one-third of the stars in the thick disc are in the 4–6 Gyr age interval, which were formed in a relatively calm, stable disc. The disc was more gas-rich and turbulent at early times, however, so the stars were formed thick 'at birth', as proposed in Bournaud et al. (2009). Furthermore, these stars continued to be kinematically heated into a thicker spatial distribution after forming. Therefore, the thick disc in our simulation is a mix of stars older than 4 Gyr, which formed through a combination of several mechanisms.

Regarding the formation of the thin disc, we note that the gas disc smoothly became thinner down to $z = 0$, thus forming the thin disc at late times. There is no sharp transition about 4 Gyr ago when the thin disc at $z = 0$ started to form.

In the literature, some authors have claimed that there is a tension between preserving thin discs and the necessity of strong stellar feedback to prevent galaxies from forming too many stars in cosmological simulations (e.g. Roškar et al. 2014). However, our simulation simultaneously forms a thin-disc component while producing a reasonable stellar mass and star formation history in good agreement with observational constraints (Hopkins et al. 2014). These results demonstrate that it is possible to form thin discs in cosmological simulations, even in the presence of strong stellar feedback. This is due to the fact that (1) our simulation has sufficient spatial resolution (smoothing length far less than the vertical scaleheights of the thin disc), (2) we allow gas to cool to very low temperatures to explicitly resolve the cold, star-forming gas, and (3) the high resolution and the physically motivated star formation and feedback models adopted in the simulation allow one to explicitly resolve the launching and venting of galactic winds without disrupting the entire

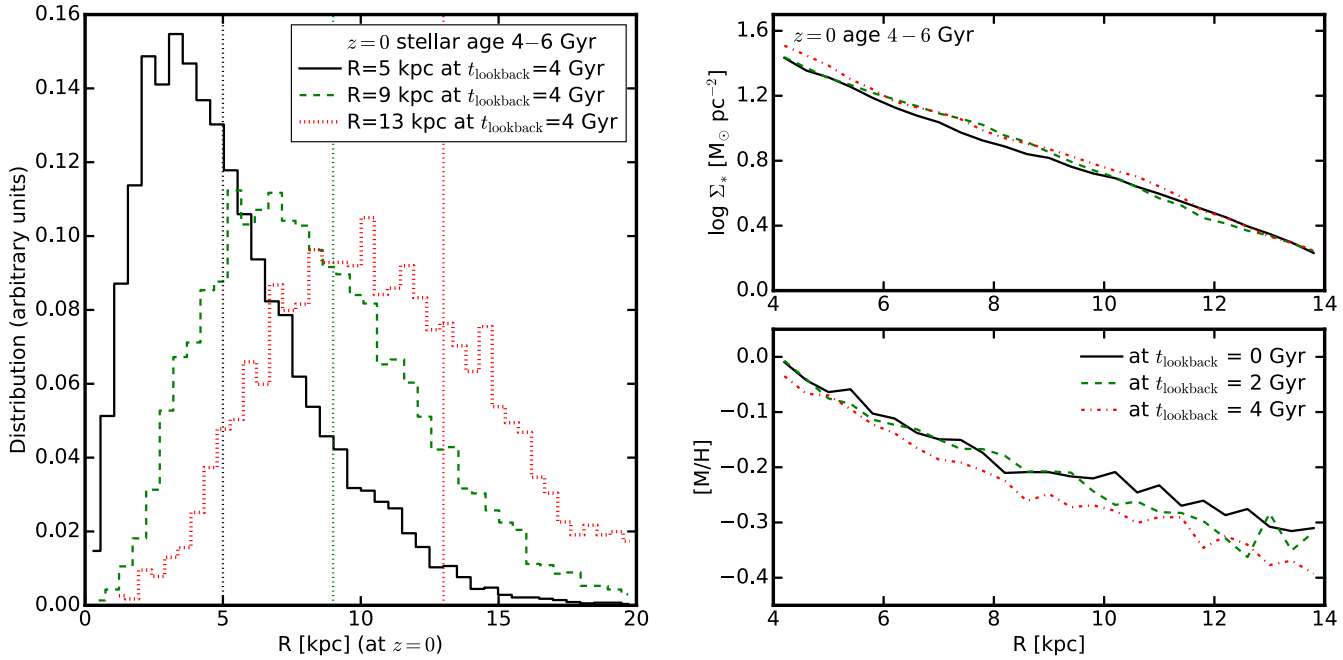

Figure 9. Left-hand panel: distribution of galactocentric radius at $z = 0$ for stars in the age interval 4–6 Gyr, which were located in three annuli centred at $R = 5$, 9 and 13 kpc (of 1-kpc width) near the disc mid-plane ($|Z| < 0.5$ kpc) at $t_{\rm lookback} = 4$ Gyr. Stars in a given annulus 4 Gyr ago have a wide distribution in R by $z = 0$. A small fraction (less than 10 per cent) of stars have migrated to very large radii ($\Delta R > 5$ kpc), while more than half of the stars have moved inwards ($\Delta R < 0$), as expected from the exchange of angular momentum. Right-hand panel: stellar surface density (top panel) and metallicity (bottom panel) profiles from $R = 4$ to 14 kpc for all stars with $z = 0$ age interval 4–6 Gyr, but measured at three epochs ($t_{\rm lookback} = 0$, 2 and 4 kpc). The surface density does not change more than 0.05 dex, while the average stellar metallicity slightly increased at large radii, but the net effect of stellar migration on the properties of a galactic disc is weak at late times, in line with the results from other simulations (e.g. Minchev et al. 2013; Grand & Kawata 2016).

galaxy. Likewise, Agertz & Kravtsov (2015, 2016) also found that their simulation can form a thin disc when using feedback recipes similar to ours but fail to do so using other feedback models.

4.2 Stellar migration in the disc

It has been proposed that radial migration of stars in the disc due to angular momentum exchange may be an important mechanism of disc heating, which also flattens the stellar metallicity gradients (e.g. Schönrich & Binney 2009a,b; Loebman et al. 2011). Recent numerical calculations suggest, however, that radial migration has a little impact on the disc thickening (e.g. Minchev et al. 2012; Martig et al. 2014b; Vera-Ciro et al. 2014; Aumer et al. 2016; Grand et al. 2016). None the less, radial migration can still occur when spiral arms and bars are present (via corotation resonance of transient spirals; e.g. Lynden-Bell & Kalnajs 1972; Sellwood & Binney 2002, or induced by long-lived spiral- or bar-like structures; e.g. Minchev & Famaey 2010; Minchev et al. 2011), while spiral arms and bars are suggested to be the dominant mechanisms of disc heating (e.g. Grand et al. 2016).

In our simulation, stars older than 8 Gyr show strong radial migration, because the bursty gas outflows driven by stellar feedback generate large fluctuations in the galactic potential, causing old stars to migrate towards large radius (El-Badry et al. 2016). This is important to shape the global structure of the disc (e.g. Minchev et al. 2015). However, this is a very different mechanism from the standard radial migration within a stable disc. To test the standard migration scenario, we study stars in the $z = 0$ age interval 4–6 Gyr. First, we go back to the snapshot at $t_{\rm lookback} = 4$ Gyr and select stars in three annuli centred at $R = 5$, 9 and 13 kpc with 1 kpc width near the disc plane ($|Z| < 0.5$ kpc) at that epoch. In the left-hand panel in Fig. 9, we show the distribution of galactocentric radius R for these stars by $z = 0$. Stars in a given annulus 4 Gyr ago have a wide distribution in R by $z = 0$. Only a small fraction (less than 10 per cent) of stars have migrated to very large radii ($\Delta R > 5$ kpc), while more than half of the stars have migrated inwards ($\Delta R < 0$). This is expected from the exchange of angular momentum between stars, because outwards-migrating stars carry more angular momentum, so more stars migrate inward. In the right-hand panel, we show the stellar surface density and metallicity profiles in $R = 4$–14 kpc for all stars with $z = 0$ age interval 4–6 Gyr, measured at three epochs ($t_{\rm lookback} = 0$, 2 and 4 Gyr). The surface density does not change by more than 0.05 dex during the past 4 Gyr (stellar mass-loss is subdominant). The average stellar metallicity has increased at large radii, resulting in a flattening of metallicity gradient by 0.01 dex kpc^{-1}. Our results suggest that radial migration is common, but only has a weak net effect on the late-time global properties (mass density, metallicity profiles) of the galactic disc, consistent with predictions from other works (e.g. Minchev et al. 2013; Grand & Kawata 2016).

4.3 Abundance patterns and MAPs

In the literature, several authors have suggested that MAPs (stars with certain [M/H] and [α/Fe]) are proxies for single-age populations in the MW (e.g. Bovy et al. 2012; Rix & Bovy 2013). This is important because one cannot infer the assembly history of the MW without reliable information on stellar ages. We first examine the abundance patterns in our simulation. In Fig. 10, we show the stellar age–metallicity relation in the left-hand panel for all stars with $R = 4$–14 kpc and $|Z| < 3$ kpc, colour-coded by the total stellar mass in each pixel (in logarithmic scale). The white dashed line

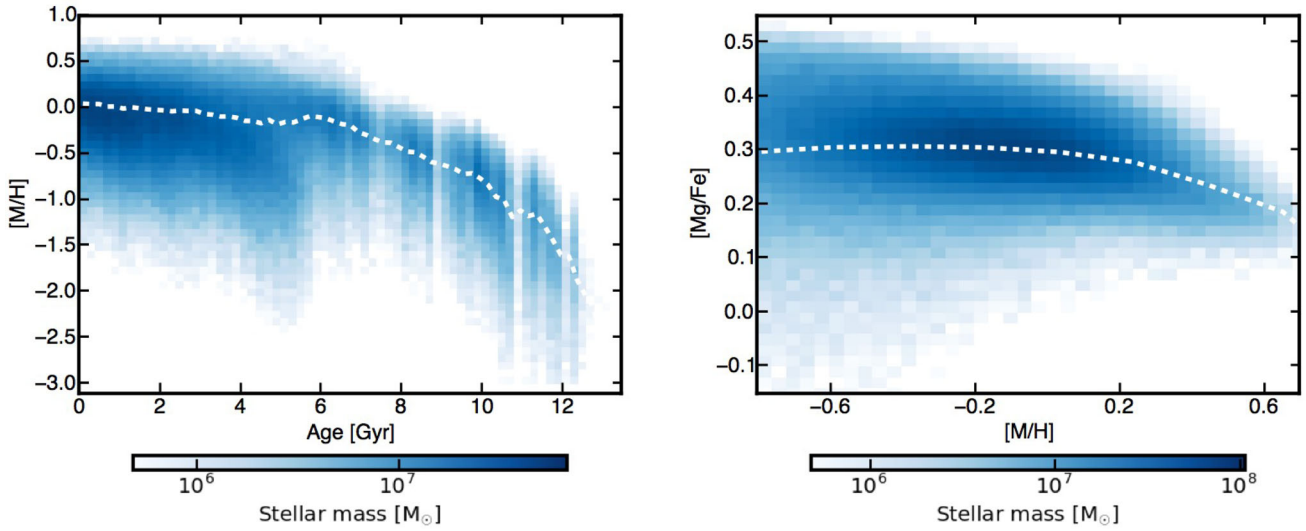

Figure 10. Left: Stellar age–metallicity relation. *Right*: [Mg/Fe]–[M/H] relation. Colours show the total stellar mass in each pixel (in logarithmic scale). The white dashed lines show the median for each relation. To leading order, stellar age, metallicity, and [Mg/Fe] correlate with each other, but there is large scatter (over 1 dex in [M/H] at a given age).

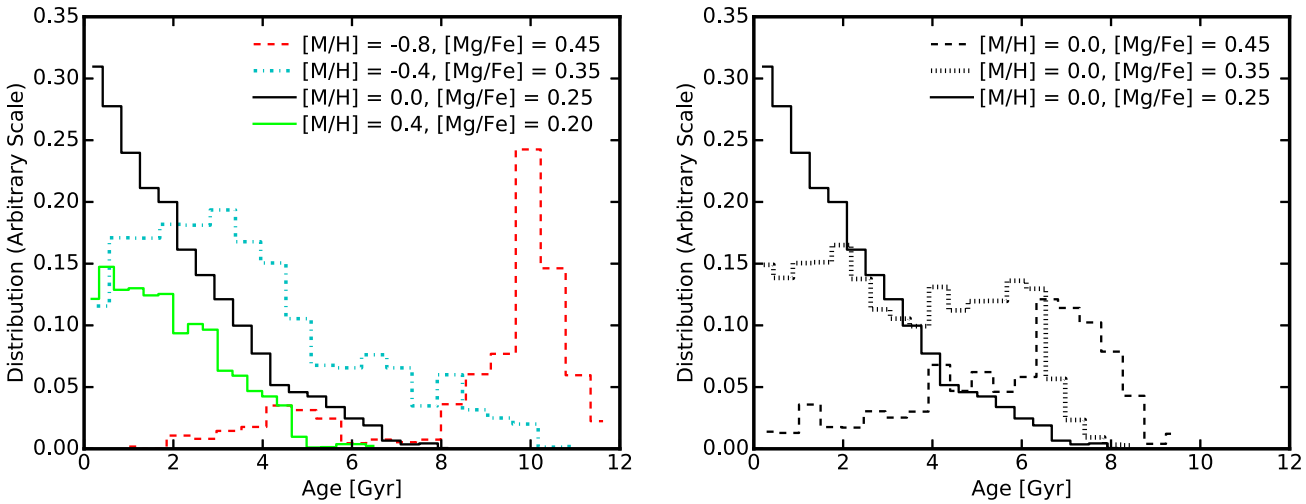

Figure 11. Stellar age distribution of six MAPs in narrow bins with Δ[M/H] = 0.06 and Δ[Mg/Fe] = 0.04. In general, metal-poor, α-rich stars represent older populations than metal-rich, α-poor stars (left-hand panel). At fixed metallicity, α-poor stars are more biased towards younger populations (right-hand panel). However, the age distribution of a MAP is wide.

shows the median relation. In the right-hand panel, we show the distributions of these stars in the [Mg/Fe]–[M/H] plane. Stellar age, metallicity and [Mg/Fe] correlate with each other to leading order, but with considerable scatter (over 1 dex in [M/H] at a given age). The scatter mainly comes from the presence of metallicity gradients in the disc and non-uniform distribution of metals in the galaxy. We have explicitly checked that including sub-resolution metal diffusion in our simulation (as in Shen, Wadsley & Stinson 2010) does not dramatically reduce the scatter.

In the left-hand panel in Fig. 11, we show the mass-weighted age distribution of stars from four MAPs selected within a tolerance in metallicity and abundance ratio of Δ[M/H] = 0.06 and Δ[Mg/Fe] = 0.04. In general, low-metallicity, α-rich populations represent old stars, while high-metallicity, α-poor stars are more biased towards younger populations. In the right-hand panel, we compare three MAPs at fixed [M/H] but different [Mg/Fe]. We find that low-α populations contain more young stars than α-rich populations. These results marginally support the idea that chemical abundances might represent stellar ages to leading order. However, we caution that for any MAP, the age distribution is wide (see also Minchev et al. 2017). For example, the most metal-poor and α-rich population still contains a non-negligible fraction of young stars with age interval 2–6 Gyr. As a consequence, if we repeat our analysis in this paper by breaking the stars into several bins of metallicity instead of stellar age, we obtain more complicated results due to age blending effects. Independent constraints on stellar age are required to break the degeneracy.

Recent observations reveal that MW stars fall into two distinct populations on the [Mg/Fe]–[M/H] plane, known as the high- and low-α populations (e.g. Adibekyan et al. 2013; Bensby et al. 2014; Anders et al. 2014; Mikolaitis et al. 2014; Nidever et al. 2014; Kordopatis et al. 2015). Such feature is difficult to explain and cannot be reproduced by current cosmological simulations (see Nidever et al. 2014, and reference therein), including ours. Nidever

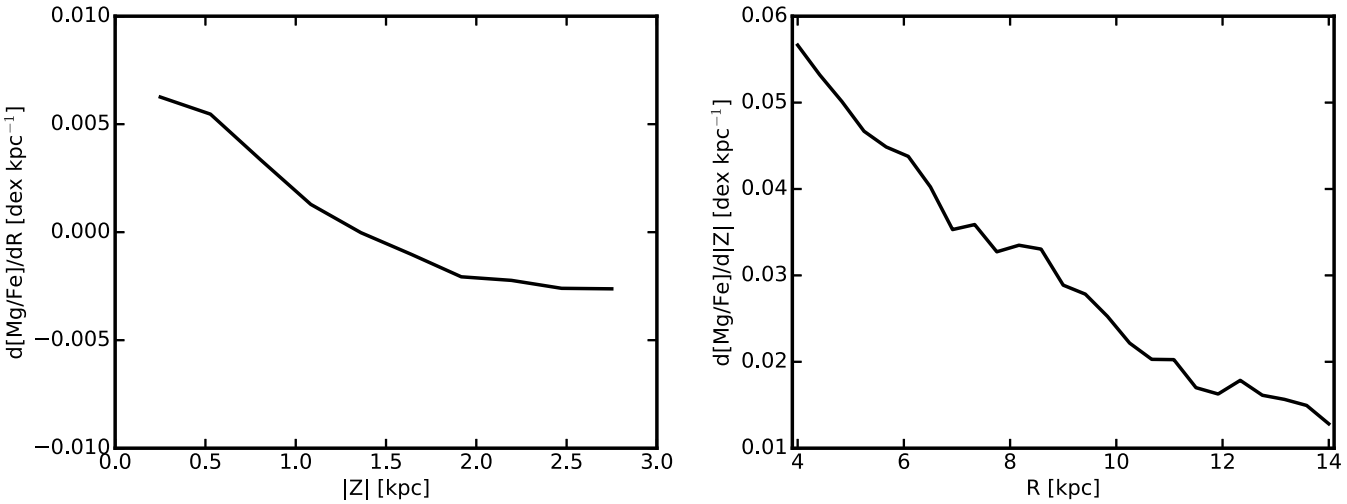

Figure 12. Left-hand panel: d[Mg/Fe]/dR as a function of $|Z|$. Right-hand panel: d[Mg/Fe]/d$|Z|$ as a function of R. The radial gradient in [Mg/Fe] is positive at the mid-plane, flattens and becomes negative at larger heights. The vertical gradient in [Mg/Fe] is positive, but is steeper at inner radii than at outer radii. These trends are similar to those of metallicity gradient, but with a flipped sign due to the anticorrelation between [Mg/Fe] and metallicity. Both of them arise from the age gradient in the disc, in line with predictions from other simulations (e.g. Minchev et al. 2013, 2014).

et al. (2014) proposed several tentative models to explain how the two populations may form, but all require fine-tuned parameters to match the observed abundance pattern. Nevertheless, we show that in our simulation, star formation has undergone two distinct modes – chaotic, bursty mode at high redshift and relatively calm, stable mode at late times. It is possible that such two-mode formation history may lead to a bimodality in the abundance pattern in very restricted conditions, while in other conditions, the two populations may simply merge. Alternatively, the MW may have a very different assembly history from our simulation. In future work, we will study a large sample of simulations of MW-size haloes with diverse assembly history and explore if and how such two populations form. Also, spectroscopic survey of stars in extragalactic galaxies with the next generation of observational facilities may also reveal whether this is common in MW-mass galaxies or just a unique feature in the MW.

4.4 [α/Fe] gradients

There is evidence indicating the presence of an [α/Fe] gradient in the MW disc (e.g. Anders et al. 2014; Boeche et al. 2014; Recio-Blanco et al. 2014), despite the fact that such measurements have large uncertainties. It is clear that the [α/Fe] gradient varies with $|Z|$ in the opposite way to [Fe/H] gradient and that d[α/Fe]/dR is negative at large $|Z|$, but the sign of d[α/Fe]/dR in the disc mid-plane is not fully consistent between various studies. Future spectroscopic surveys that include much larger samples will provide a more robust measurement. Here we use our simulation to make qualitative predictions for [α/Fe] gradients. In Fig. 12, we show the radial gradient of [Mg/Fe] as a function of height $|Z|$ (left-hand panel) and the vertical gradient of [Mg/Fe] as a function of radius R (right-hand panel). We find that d[Mg/Fe]/dR is positive near the mid-plane, gradually decreases to zero at about $|Z| = 1.3$ kpc and turns negative at larger heights. Moreover, d[Mg/Fe]/d$|Z|$ is positive at all radii, but is larger at the inner disc than at the outer disc. These are qualitatively similar to the trends of metallicity gradient presented in Section 3.3, with the sign flipped following the anticorrelation between [Mg/Fe] and [M/H], as found also in other simulations (e.g. Minchev et al. 2013, 2014). The gradient of [Mg/Fe] is also a consequence of the age gradient in the disc.

5 CONCLUSIONS

In this work, we have studied the structure, age and metallicity gradients, and dynamical evolution of the stellar disc via a case study of one simulation from the FIRE project, chosen to be a disc galaxy of similar mass to the MW at $z = 0$. The simulation is a cosmological zoom-in simulation that includes physically motivated models of the multiphase ISM, star formation and stellar feedback, with parameters taken directly from stellar evolution models. Our main findings include the following:

(i) Stars older than 6 Gyr (formation redshift $z \gtrsim 0.7$) were formed in a violent, bursty mode in a clumpy galaxy progenitor with powerful episodic outflows, and thus have round, puffy morphologies at $z = 0$. Stars younger than 6 Gyr were formed in a relatively calm, well-maintained star-forming disc. By $z = 0$, stars that formed in the chaotic mode have the largest scaleheights. Even for those that formed in a disc at late times, their scaleheights increase with stellar age at any radius; stars of the same age have larger scaleheights in the outer disc than in the inner disc (flaring). As a consequence, the median stellar age increases with $|Z|$ at a fixed radius, but decreases with R in a constant-$|Z|$ layer.

(ii) The radial metallicity gradient is negative at the mid-plane, gradually flattens when moving to larger $|Z|$, and ultimately turns positive at about $|Z| > 1.5$ kpc. The vertical metallicity gradient is negative at all radii, but is stronger at small radii. These trends are qualitatively consistent with observations in the MW. Such variation of metallicity gradient naturally follows the age gradient in the disc, since stellar age, metallicity and [α/Fe] all correlate with each other. Similar trends also exist in [α/Fe] gradients, but with a flipped sign due to the anticorrelation between [α/Fe] and metallicity.

(iii) For stars that formed within the past 6 Gyr, in a disc, those that formed earlier were thicker 'at birth' than those that formed later, because the star-forming disc was more gas-rich and therefore more turbulent and thicker at earlier times (a factor of $\sim$2 thicker at 6 Gyr ago). After each population formed, their scaleheight was

further increased via kinematic heating (by ∼40 per cent during the past 6 Gyr). In our simulation, the two factors have a comparable effect in absolute units on the differential scaleheights by $z = 0$.

(iv) The vertical stellar density at $z = 0$ can be well described by a two-component profile, defined as the traditional 'thin disc' (scaleheight $Z_H \sim 200$–500 pc) and 'thick disc' ($Z_H \sim 1$–1.5 kpc). The thin and thick discs can be roughly separated by stars younger and older than 4 Gyr. Two-third of the stars in the thick disc are formed during the chaotic, bursty phase; the other one-third stars in the thick disc are formed in a gas-rich star-forming disc and then were further thickened via kinematic heating. The gas disc smoothly evolves during the past 6 Gyr and forms the thin disc at late times. Therefore, the thick disc is a mix of stars that formed via different mechanisms, while the formation is continuous at the transition time (around 4 Gyr ago) when the $z = 0$ thin-disc stars started to form.

(v) Our simulation demonstrates that it is possible to form a thin disc in sufficiently high-resolution cosmological simulations, even in the presence of a strong stellar feedback.

Although we study only one simulation in this paper, our main results here are derived from global processes that can be understood with simple analytic arguments, including the following: (1) Star formation is bursty at high redshift and becomes relatively stable at late times, (2) the thickness of the star-forming gas disc decreases at low gas fraction, and (3) kinematic heating is continuously present from spiral structure, bars, GMCs, etc. In fact, some of our results agree very well with previous studies by other authors. For instance, almost all simulations of MW analogues show violent merger history at high redshift but relatively quiescent merger history at late times. Most of them form a separate thin and thick disc by $z = 0$, with their scaleheights and mass fractions similar to ours (e.g. Brook et al. 2012; Bird et al. 2013; Minchev et al. 2013; Martig et al. 2014a). Some models also successfully reproduce the observed MW abundance distribution and the variation of stellar metallicity gradients, and attribute these results to the disc formation history (e.g. Minchev et al. 2013, 2014). Therefore, our results further confirm that the physical processes we proposed are common in the assembly histories of disc galaxies, regardless of numerical details and feedback model.

One key prediction of our simulation is that the thick disc does *not* form from a single channel, but it is rather a mixture of stars that formed and evolved in three different ways [see conclusion (iv) and Section 4.1 for details]. This scenario can be tested by future observations of MW stars if an independent constraint on stellar age can be obtained. For example, we expect that the age separation between thin- and thick-disc stars is different from the one between stars that formed in the chaotic mode and in the calm mode. The latter can be identified by a sudden jump in the velocity dispersion as a function of stellar age.

Nevertheless, our simulation is not designed or chosen in any way to be identical to the MW and differs from it in several aspects. The radial metallicity gradient is -0.03 dex kpc^{-1} in the disc midplane in our simulation, shallower than the -0.06 dex kpc^{-1} slope in the MW disc (e.g. Cheng et al. 2012). This can be affected by disc scalelength, disc pre-enrichment at formation time, the extent of radial mixing, and specific merger or accretion events in the past. Also, our simulation does not show any bimodality in the [α/Fe]–[M/H] relation, in contrast to some observations of MW stars (e.g. Nidever et al. 2014). Moreover, our simulation does not show a prominent central bar, with which we expect that kinematic heating would be stronger (e.g. Grand et al. 2016). Such differences may originate from details in the assembly history. In future work, we will further explore the disc formation, morphology, and metallicity profile and their dependence on galaxy formation history using an enlarged sample of disc galaxy simulations.

ACKNOWLEDGEMENTS

We thank David Nidever, Hans-Walter Rix, Charlie Conroy and Paul Torrey for useful discussions. We also acknowledge Oscar Agertz and Ivan Minchev for helpful comments after the first draft has appeared on arXiv, and the anonymous referee for a detailed report. The simulations used in this paper were run on XSEDE computational resources (allocations TG-AST120025, TG-AST130039 and TG-AST140023). The analysis was performed on the Caltech compute cluster 'Zwicky' (NSF MRI award #PHY-0960291). Support for PFH was provided by an Alfred P. Sloan Research Fellowship, NASA ATP Grant NNX14AH35G, and NSF Collaborative Research Grant #1411920 and CAREER grant #1455342. ARW was supported by a Caltech-Carnegie Fellowship, in part through the Moore Center for Theoretical Cosmology and Physics at Caltech. DAA acknowledges support by a CIERA Postdoctoral Fellowship. C-AF-G was supported by NSF through grants AST-1412836 and AST-1517491, by NASA through grant NNX15AB22G, and by STScI through grants HST-AR-14293.001-A and HST-GO-14268.022-A. DK was supported by NSF grant AST-1412153 and funds from the University of California, San Diego. EQ was supported by NASA ATP grant 12-APT12-0183, by a Simons Investigator award from the Simons Foundation, and by the David and Lucile Packard Foundation.

REFERENCES

Abadi M. G., Navarro J. F., Steinmetz M., Eke V. R., 2003, ApJ, 597, 21
Adibekyan V. Z. et al., 2013, A&A, 554, A44
Agertz O., Kravtsov A. V., 2015, ApJ, 804, 18
Agertz O., Kravtsov A. V., 2016, ApJ, 824, 79
Allaert F. et al., 2015, A&A, 582, A18
Allende Prieto C. et al., 2008, Astron. Nachr., 329, 1018
Anders F. et al., 2014, A&A, 564, A115
Anglés-Alcázar D., Faucher-Giguère C.-A., Kereš D., Hopkins P. F., Quataert E., Murray N., 2016, preprint (arXiv:1610.08523)
Aumer M., Binney J., Schönrich R., 2016, MNRAS, 459, 3326
Bensby T., Feltzing S., Oey M. S., 2014, A&A, 562, A71
Bird J. C., Kazantzidis S., Weinberg D. H., Guedes J., Callegari S., Mayer L., Madau P., 2013, ApJ, 773, 43
Boeche C. et al., 2013, A&A, 559, A59
Boeche C. et al., 2014, A&A, 568, A71
Bournaud F., Elmegreen B. G., Martig M., 2009, ApJ, 707, L1
Bovy J., Rix H.-W., Liu C., Hogg D. W., Beers T. C., Lee Y. S., 2012, ApJ, 753, 148
Bovy J., Rix H.-W., Schlafly E. F., Nidever D. L., Holtzman J. A., Shetrone M., Beers T. C., 2016, ApJ, 823, 30
Brook C. B., Kawata D., Gibson B. K., Freeman K. C., 2004, ApJ, 612, 894
Brook C. B. et al., 2012, MNRAS, 426, 690
Bryan G. L., Norman M. L., 1998, ApJ, 495, 80
Carlberg R. G., 1987, ApJ, 322, 59
Carrell K., Chen Y., Zhao G., 2012, AJ, 144, 185
Cheng J. Y. et al., 2012, ApJ, 746, 149
Chiappini C., Matteucci F., Gratton R., 1997, ApJ, 477, 765
Comerón S. et al., 2011, ApJ, 729, 18
Comerón S. et al., 2012, ApJ, 759, 98
El-Badry K., Wetzel A., Geha M., Hopkins P. F., Kereš D., Chan T. K., Faucher-Giguère C.-A., 2016, ApJ, 820, 131
Faucher-Giguère C.-A., Lidz A., Zaldarriaga M., Hernquist L., 2009, ApJ, 703, 1416

Faucher-Giguère C.-A., Kereš D., Dijkstra M., Hernquist L., Zaldarriaga M., 2010, ApJ, 725, 633
Faucher-Giguère C.-A., Quataert E., Hopkins P. F., 2013, MNRAS, 433, 1970
Faucher-Giguère C.-A., Hopkins P. F., Kereš D., Muratov A. L., Quataert E., Murray N., 2015, MNRAS, 449, 987
Faucher-Giguère C.-A., Feldmann R., Quataert E., Kereš D., Hopkins P. F., Murray N., 2016, MNRAS, 461, L32
Faure C., Siebert A., Famaey B., 2014, MNRAS, 440, 2564
Feldmann R., Hopkins P. F., Quataert E., Faucher-Giguère C.-A., Kereš D., 2016, MNRAS, 458, L14
Fuhrmann K., 1998, A&A, 338, 161
Gilmore G., Reid N., 1983, MNRAS, 202, 1025
Gilmore G. et al., 2012, The Messenger, 147, 25
Gómez F. A., Minchev I., O'Shea B. W., Beers T. C., Bullock J. S., Purcell C. W., 2013, MNRAS, 429, 159
Grand R. J. J., Kawata D., 2016, Astron. Nachr., 337, 957
Grand R. J. J., Springel V., Gómez F. A., Marinacci F., Pakmor R., Campbell D. J. R., Jenkins A., 2016, MNRAS, 459, 199
Gregersen D. et al., 2015, AJ, 150, 189
Hafen Z. et al., 2016, preprint (arXiv:1608.05712)
Hayden M. R. et al., 2014, AJ, 147, 116
Hayward C. C., Hopkins P. F., 2017, MNRAS, 465, 1682
Haywood M., Di Matteo P., Lehnert M. D., Katz D., Gómez A., 2013, A&A, 560, A109
Hinshaw G. et al., 2013, ApJS, 208, 19
Ho I.-T., Kudritzki R.-P., Kewley L. J., Zahid H. J., Dopita M. A., Bresolin F., Rupke D. S. N., 2015, MNRAS, 448, 2030
Hopkins P. F., 2013, MNRAS, 428, 2840
Hopkins P. F., 2015, MNRAS, 450, 53
Hopkins P. F., Hernquist L., Cox T. J., Younger J. D., Besla G., 2008, ApJ, 688, 757
Hopkins P. F., Narayanan D., Murray N., 2013, MNRAS, 432, 2647
Hopkins P. F., Kereš D., Oñorbe J., Faucher-Giguère C.-A., Quataert E., Murray N., Bullock J. S., 2014, MNRAS, 445, 581
Iwamoto K., Brachwitz F., Nomoto K., Kishimoto N., Umeda H., Hix W. R., Thielemann F.-K., 1999, ApJS, 125, 439
Izzard R. G., Tout C. A., Karakas A. I., Pols O. R., 2004, MNRAS, 350, 407
Kalberla P. M. W., Kerp J., Dedes L., Haud U., 2014, ApJ, 794, 90
Kazantzidis S., Bullock J. S., Zentner A. R., Kravtsov A. V., Moustakas L. A., 2008, ApJ, 688, 254
Kennicutt R. C., Jr, 1998, ARA&A, 36, 189
Kim J.-h. et al., 2014, ApJS, 210, 14
Knollmann S. R., Knebe A., 2009, ApJS, 182, 608
Kordopatis G. et al., 2015, A&A, 582, A122
Kroupa P., 2002, Science, 295, 82
Leitherer C. et al., 1999, ApJS, 123, 3
Loebman S. R., Roškar R., Debattista V. P., Ivezić Ž., Quinn T. R., Wadsley J., 2011, ApJ, 737, 8
López-Corredoira M., Molgó J., 2014, A&A, 567, A106
Lynden-Bell D., Kalnajs A. J., 1972, MNRAS, 157, 1
Ma X., Hopkins P. F., Faucher-Giguère C.-A., Zolman N., Muratov A. L., Kereš D., Quataert E., 2016, MNRAS, 456, 2140
Ma X., Hopkins P. F., Feldmann R., Torrey P., Faucher-Giguere C.-A., Keres D., 2017, MNRAS, 466, 4780
Mannucci F., Della Valle M., Panagia N., 2006, MNRAS, 370, 773
Maoz D., Sharon K., Gal-Yam A., 2010, ApJ, 722, 1879
Martig M., Minchev I., Flynn C., 2014a, MNRAS, 442, 2474
Martig M., Minchev I., Flynn C., 2014b, MNRAS, 443, 2452
Martig M., Minchev I., Ness M., Fouesneau M., Rix H.-W., 2016, ApJ, 831, 139
Matteucci F., Brocato E., 1990, ApJ, 365, 539
Mikolaitis Š. et al., 2014, A&A, 572, A33
Minchev I., Famaey B., 2010, ApJ, 722, 112
Minchev I., Quillen A. C., 2006, MNRAS, 368, 623
Minchev I., Famaey B., Combes F., Di Matteo P., Mouhcine M., Wozniak H., 2011, A&A, 527, A147
Minchev I., Famaey B., Quillen A. C., Dehnen W., Martig M., Siebert A., 2012, A&A, 548, A127
Minchev I., Chiappini C., Martig M., 2013, A&A, 558, A9
Minchev I., Chiappini C., Martig M., 2014, A&A, 572, A92
Minchev I., Martig M., Streich D., Scannapieco C., de Jong R. S., Steinmetz M., 2015, ApJ, 804, L9
Minchev I., Steinmetz M., Chiappini C., Martig M., Anders F., Matijevic G., de Jong R. S., 2017, MNRAS, 834, 27
Miranda M. S. et al., 2016, A&A, 587, A10
Momany Y., Zaggia S., Gilmore G., Piotto G., Carraro G., Bedin L. R., de Angeli F., 2006, A&A, 451, 515
Muratov A. L., Kereš D., Faucher-Giguère C.-A., Hopkins P. F., Quataert E., Murray N., 2015, MNRAS, 454, 2691
Muratov A. L. et al., 2016, preprint (arXiv:1606.09252)
Nidever D. L. et al., 2014, ApJ, 796, 38
Nomoto K., Tominaga N., Umeda H., Kobayashi C., Maeda K., 2006, Nucl. Phys. A, 777, 424
Nordström B. et al., 2004, A&A, 418, 989
O'Brien J. C., Freeman K. C., van der Kruit P. C., 2010, A&A, 515, A62
Olling R. P., 1995, AJ, 110, 591
Orr M. et al., 2017, preprint (arXiv:1701.01788)
Planck Collaboration XVI, 2014, A&A, 571, A16
Price D. J., Monaghan J. J., 2007, MNRAS, 374, 1347
Purcell C. W., Kazantzidis S., Bullock J. S., 2009, ApJ, 694, L98
Purcell C. W., Bullock J. S., Tollerud E. J., Rocha M., Chakrabarti S., 2011, Nature, 477, 301
Qu Y., Di Matteo P., Lehnert M. D., van Driel W., 2011, A&A, 530, A10
Quinn P. J., Hernquist L., Fullagar D. P., 1993, ApJ, 403, 74
Recio-Blanco A. et al., 2014, A&A, 567, A5
Rix H.-W., Bovy J., 2013, A&AR, 21, 61
Roškar R., Teyssier R., Agertz O., Wetzstein M., Moore B., 2014, MNRAS, 444, 2837
Saha K., Tseng Y.-H., Taam R. E., 2010, ApJ, 721, 1878
Schönrich R., Binney J., 2009a, MNRAS, 396, 203
Schönrich R., Binney J., 2009b, MNRAS, 399, 1145
Sellwood J. A., Binney J. J., 2002, MNRAS, 336, 785
Sellwood J. A., Carlberg R. G., 1984, ApJ, 282, 61
Shen S., Wadsley J., Stinson G., 2010, MNRAS, 407, 1581
Sparre M., Hayward C. C., Feldmann R., Faucher-Giguère C.-A., Muratov A. L., Kereš D., Hopkins P. F., 2017, MNRAS, 466, 88
Spitzer L., Jr, Schwarzschild M., 1951, ApJ, 114, 385
Spitzer L., Jr, Schwarzschild M., 1953, ApJ, 118, 106
Steinmetz M. et al., 2006, AJ, 132, 1645
Stinson G. S. et al., 2013, MNRAS, 436, 625
Thompson T. A., Quataert E., Murray N., 2005, ApJ, 630, 167
van de Voort F., Quataert E., Hopkins P. F., Kereš D., Faucher-Giguère C.-A., 2015, MNRAS, 447, 140
Vera-Ciro C., D'Onghia E., Navarro J., Abadi M., 2014, ApJ, 794, 173
Villalobos Á., Helmi A., 2008, MNRAS, 391, 1806
Wetzel A. R., Hopkins P. F., Kim J.-h., Faucher-Giguère C.-A., Kereš D., Quataert E., 2016, ApJ, 827, L23
Wiersma R. P. C., Schaye J., Smith B. D., 2009a, MNRAS, 393, 99
Wiersma R. P. C., Schaye J., Theuns T., Dalla Vecchia C., Tornatore L., 2009b, MNRAS, 399, 574
Woosley S. E., Weaver T. A., 1995, ApJS, 101, 181
Yanny B. et al., 2009, AJ, 137, 4377
Yoachim P., Dalcanton J. J., 2006, AJ, 131, 226
Yurin D., Springel V., 2015, MNRAS, 452, 2367

APPENDIX A: RESOLUTION TEST

In this paper, we performed a case study of a cosmological zoom-in simulation that produces a MW-mass disc galaxy at $z = 0$. This simulation is originally presented in Hopkins et al. (2014) and has been thoroughly studied in other works (Faucher-Giguère et al. 2015; Muratov et al. 2015; van de Voort et al. 2015; El-Badry et al. 2016; Ma et al. 2016, 2017). Recently, Wetzel et al. (2016) have re-run

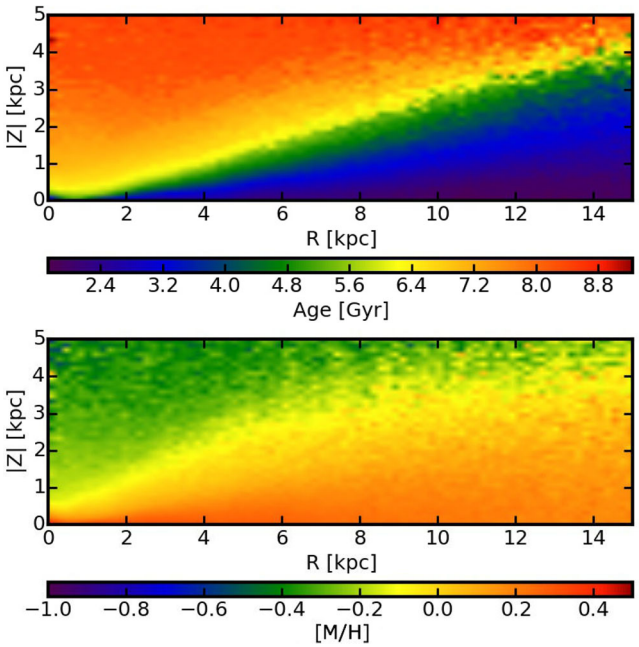

Figure A1. The same as Fig. 4, but for the ultra-high-resolution simulation presented in Wetzel et al. (2016). The disc structure does not significantly differ from the simulation studied in this paper, although this run has an eight times better mass resolution and uses a more accurate hydrodynamic solver.

this simulation with an eight times better mass resolution and a higher spatial resolution ($\epsilon_{\rm gas} = 1\,$pc and $\epsilon_{\rm star} = 4\,$pc), but using the meshless finite-mass hydrodynamics method in GIZMO and FIRE-2, an improved numerical implementation of the FIRE model (see Hopkins et al., in preparation, for details). We repeat our analysis on the new run and find all the results presented in this paper remain qualitatively unchanged. Particularly, the thin-to-thick disc decomposition, disc scaleheights and the amount of disc thickening at late times are consistent within 10 per cent. As one explicit example, in Fig. A1, we show the median stellar age and average stellar metallicity as a function of R and $|Z|$ in the new run. The disc structure and metallicity profile are very similar to the simulation analysed in this paper (Fig. 4). This suggests that our results are independent of resolution and numerical details, because most of the physics we consider in this paper are global processes and can be understood by simple analytic considerations. Nevertheless, there are some quantitative differences between the two runs. In the new run, the star-forming disc formed and stabilized at a later time ($t_{\rm lookback} \sim 4\,$Gyr), due to stochastic effects during the last minor merger. The gas disc is more metal-enriched at formation time, so the radial metallicity gradient on the mid-plane is weaker. Moreover, the disc is more strongly flared, so the radial metallicity gradient turns positive at a lower height ($|Z| \sim 1\,$kpc). This suggests that a large statistical sample is needed to make rigorous statements about quantitative details, as opposed to the robust qualitative trends we have focused on here.

This paper has been typeset from a TEX/LATEX file prepared by the author.